Oncogene
https://doi.org/10.1038/s41388-019-1033-x

ARTICLE

ΔNp63α exerts antitumor functions in cervical squamous cell carcinoma

Ying Zhou[1] · Hanyuan Liu[2] · Juan Wang[2] · Xiaolin Wang[3] · Lili Qian[1] · Fei Xu[2] · Weiguo Song[2] · Dabao Wu[1] · Zhen Shen[1] · Dingqing Feng[4] · Bin Ling[4] · Weihua Xiao[3] · Ge Shan[3,5] · Liang Chen[1,3]

Received: 12 October 2018 / Revised: 16 September 2019 / Accepted: 19 September 2019

Abstract

The molecular basis underlying the aggressive nature and excessive proliferation of cervical squamous cancer cell remains unclear. ΔNp63α is the predominant isotype of p63 expressed in the epithelia and regulates epithelial cell differentiation. The pro-/anti-tumor role of ΔNp63α in different kinds of solid tumors remains controversial and the precise molecular mechanisms are still elusive. In this study, we uncovered the molecular functions of ΔNp63α in cervical squamous cell carcinoma to clarify its roles as a tumor suppressor. We demonstrated that ΔNp63α suppressed cell migration, invasiveness, and tumor growth in SiHa and ME-180 cells with both in vivo and in vitro assays. Mechanistic investigation via RNA-sequencing and chromatin immunoprecipitation-sequencing revealed that ΔNp63α exerted its antitumor capacity via regulating the expression of a cohort of cell junction genes. Further, we showed that ZNF385B and CLDN1 were two direct ΔNp63α targets with significant relevance to cervical squamous cell carcinoma examined in cell cultures, tumor xenografts, and clinic tumors. We also demonstrated that ΔNp63α downregulated NFATC1 to reduce cisplatin resistance. These findings shed new lights on functions of ΔNp63α in tumors and providing novel insights in targeted therapy of cervical cancers.

Introduction

Cervical squamous cell carcinoma (CSCC) is an aggressive malignancy arising within the stratified epithelium of the cervix [1]. According to the cancer statistics in 2017, cervical cancers (~90% of them are CSCCs) rank no. 2 of cancer death in women aged 20–39 [2]. It is known that abnormal regenerative proliferation and blocked differentiation are vital drivers of squamous tumors including CSCC [3]. Human papillomavirus (HPV) has been identified as the key agent to cause these abnormalities in ~99% of the cancers in uterine cervix [4]. HPV infection often leads to aberrant expression of genes such as KLF5, TPRG1, and TP63 due to the genomic insertion of HPV or other mechanisms [5]. Chemotherapy of CSCC is generally conducted by cisplatin or cisplatin plus fluorouracil [6, 7].

These authors contributed equally: Ying Zhou, Hanyuan Liu

Significance: ΔNp63α functions as a tumor suppressor in CSCC by regulating the expression of a cohort of cell junction genes and some other target genes such as CLDN1, ZNF385B, and NFATC1.

Supplementary information The online version of this article (https://doi.org/10.1038/s41388-019-1033-x) contains supplementary material, which is available to authorized users.

✉ Ge Shan
shange@ustc.edu.cn

✉ Liang Chen
anqingcl@ustc.edu.cn

[1] Department of Obstetrics and Gynecology, The First Affiliated Hospital of University of Science & Technology of China, Anhui Provincial Hospital, Hefei, 230001 Anhui Province, China

[2] Anhui Medical University, Hefei, 230001 Anhui Province, China

[3] Division of Molecular Medicine, Hefei National Laboratory for Physical Sciences at Microscale, the CAS Key Laboratory of Innate Immunity and Chronic Disease, School of Life Sciences, University of Science and Technology of China, 230027 Hefei, China

[4] Department of Obstetrics and Gynecology, Peking Union Medical College Hospital, Peking Union Medical College & Chinese Academy of Medical Sciences, 100730 Beijing, China

[5] CAS Centre for Excellence in Molecular Cell Science, Shanghai Institutes for Biological Sciences, CAS, 200031 Shanghai, China

Published online: 01 October 2019

TP63 encodes a crucial transcription factor p63, which is a member of the p53 family and plays critical roles in regulating epithelial development [8, 9]. p63 has three isoforms according to different promoters, TA, ΔN, and GTA (germ cell-encoded trans-activating p63). TA and ΔN isoforms generate variants such as α, β, γ, and δ due to alternative splicing at the carboxy terminal [10]. Notably, the TAp63 isoforms, due to their transactivation domain, are capable of trans-activating a set of genes shared with those of p53, such as BAX and MDM2.

ΔNp63α, however, lacks the majority of the transactivation domain but still has transactivation activity [11]. In addition, the ΔNp63α can inhibit the function of p53 family members through forming protein complexes with p53 family proteins [11]. Also, ΔNp63α is the major isotype controlling epithelium morphogenesis [9–12]. Aberrant expression of ΔNp63α can interrupt normal differentiation, promote survival of epithelial cells, and contribute to malignant transformation through various mechanisms [13].

Till now, it is controversial for roles of ΔNp63α in cancers [14–16]. Some reports showed that higher levels of ΔNp63α could promote cancer cell proliferation and invasion, and lead to chemotherapeutic resistance through various mechanisms in many tumors such as primary head and neck squamous cell carcinomas, breast cancer, and non-small cell lung cancer [17–22]. Some other studies suggested the role of ΔNp63α in metastasis prevention, inhibition of epithelial–mesenchymal transition, induction of cell cycle arrest, apoptosis, and regulation of p53 target genes [23–25]. Taken together, the effects of ΔNp63α might rely heavily on tumor and tissue specificity.

We and others have demonstrated that ΔNp63α is the predominant isotype expressed in the cervix, while other isotypes are hardly detectable. [25, 26]. ΔNp63α has decreased expression levels in CSCC, although there have been no systematic analyses for ΔNp63α downstream genes in CSCC [26, 27].

To further investigate the roles of ΔNp63α in CSCC, we sought to identify the targets of ΔNp63α, and to dissect molecular pathways that dictated by ΔNp63α in CSCC. In this study, we have identified target genes of ΔNp63α by RNA-sequencing (RNA-seq) and chromatin immunoprecipitation followed with deep sequencing (ChIP-seq) in cervical cancerous cells. We have revealed that ΔNp63α plays a central role in regulating cell junction genes in CSCC. Further analysis and examinations with in vivo and in vitro experiments have demonstrated that ΔNp63α has antitumor effects by regulating critical targets such as ZNF385B and CLDN1, and ΔNp63α also inhibits the expression of NFATC1 to reduce cisplatin resistance in CSCC.

Results

ΔNp63α reduces proliferation of cervical squamous carcinoma cells in vitro and in vivo

To further investigate the functions of ΔNp63α in cervical squamous tumorigenesis, we screened four cervical squamous cancer cell lines (ME-180 and MS751 with high expression of ΔNp63α, HeLa, and SiHa with low expression of ΔNp63α) (Supplementary Fig. S1A). ME-180 and MS751 cells exhibited significant reduction of cell proliferation, colony formation, and migration. On the other hand, HeLa and SiHa cells displayed significantly higher capability of cell proliferation, colony formation, and migration (Supplementary Fig. S1B–D). We selected SiHa (low expression of ΔNp63α) and ME-180 (high expression of ΔNp63α) for in-depth study (Fig. 1a). We then established stable SiHa cells with the overexpression of ΔNp63α (SiHa/p63), and stable ME-180 cells with ΔNp63α shRNA knockdown (ME-180/shp63) (Fig. 1b). Compared with control, cell proliferation (Fig. 1c) and colony formation were significantly reduced in SiHa/p63 cells (Fig. 1d). On the other hand, cell proliferation and colony formation were significantly increased in ME-180/shp63 cells compared with the control (Fig. 1c, d). Cell cycle distribution analysis further showed that more cells stayed in G0/G1 phase in SiHa/p63 cells, while fewer cells stayed in G0/G1 phase in ME-180/shp63 cells (Fig. 1e).

We then examined whether ΔNp63α regulated tumorigenesis of cervical carcinoma cells in vivo. SiHa/p63, ME-180/shp63, and their corresponding control cells were subcutaneously injected into nude mice. The ΔNp63α expression levels in dissected tumors were later confirmed in tissue section slides by immunohistochemistry staining (Supplementary Fig. S2A, B). The tumors from SiHa/p63 cells grew significantly slower than those from control cells (Fig. 2a). On the other hand, tumors in the ME-180/shp63 group grew significantly faster as compared with its control (Fig. 2b). The SiHa/p63-derived tumors were further confirmed through immunohistochemistry staining. Compared with the control, SiHa/p63-derived tumors exhibited lower levels of Ki-67, total STAT3, Y705-pSTAT3, and Survivin and higher levels of K5 (Keratin 5) and Involucrin (Fig. 2c). Compared with their controls, ME-180/shp63-derived tumors showed higher levels of Ki-67, total STAT3, active STAT3 (Y705-pSTAT3), and with Survivin, and lower levels of K5 and Involucrin (Fig. 2d). Notably, the antibody used for total STAT3 may only be suitable to evaluate the total amount of STAT3 proteins, but not very good for evaluate cytoplasmic/nuclear localization of STAT3 (Fig. 2c, d). Phospho-STAT3 staining together with the total STAT3 staining demonstrated the negative association between active STAT3 and p63 levels. The in vivo effect of ΔNp63α on metastasis of CSCC requires

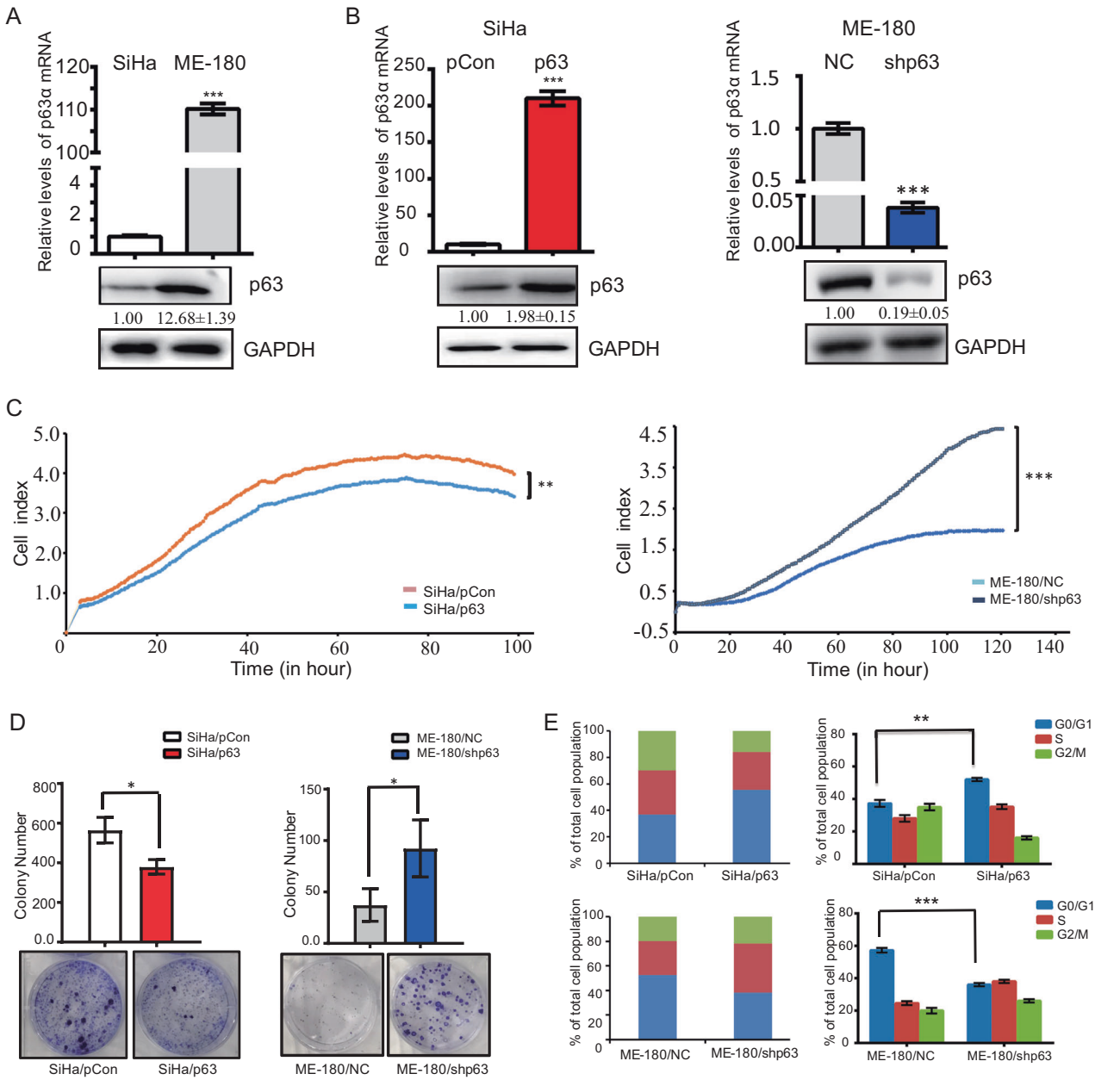

Fig. 1 ΔNp63α inhibits proliferation of cervical squamous cells in vitro. **a** ΔNp63α mRNA levels (upper) and protein levels (lower) in SiHa and ME-180 cells. **b** mRNA and protein levels of ΔNp63α in SiHa/p63 (SiHa cells with stable overexpression of ΔNp63α), and ME-180/shp63 (ME-180 cells with knockdown of ΔNp63α) cells. **c** Proliferation curves of SiHa/p63 cells (left) and ME-180/shp63 cells (right) compared with the corresponding controls, respectively. **d** Colony formation assays of SiHa/p63 and ME-180/shp63 cells. **e** Cell cycle distribution analyses of SiHa/p63 cells (upper) and ME-180/shp63 cells (lower). All the experiments were performed in triplicates. Error bars, SD, data are means ± SEM. n.s., not significant, $*p < 0.05$, $**p < 0.01$, $***p < 0.001$, are based on the Student's *t*-test

further investigations. In summary, higher levels of ΔNp63α could suppress tumorigenesis in CSCC, while lower levels of ΔNp63α would promote tumorigenesis in CSCC.

ΔNp63α regulates epithelial–mesenchymal transition in cervical squamous carcinoma cells

It is known that epithelial–mesenchymal transition plays crucial roles during development and also in the tumor invasion process [28, 29]. To investigate whether ΔNp63α regulated epithelial–mesenchymal transition in CSCC, we examined the expression of epithelial and mesenchymal markers by western blot and immunohistochemistry. We found that ΔNp63α overexpression increased the levels of epithelial markers (E-cadherin and β-catenin) and decreased the levels of mesenchymal markers (N-cadherin and vimentin) both in vitro and in vivo (Fig. 3a, b). ΔNp63α knockdown resulted in the downregulation of epithelial

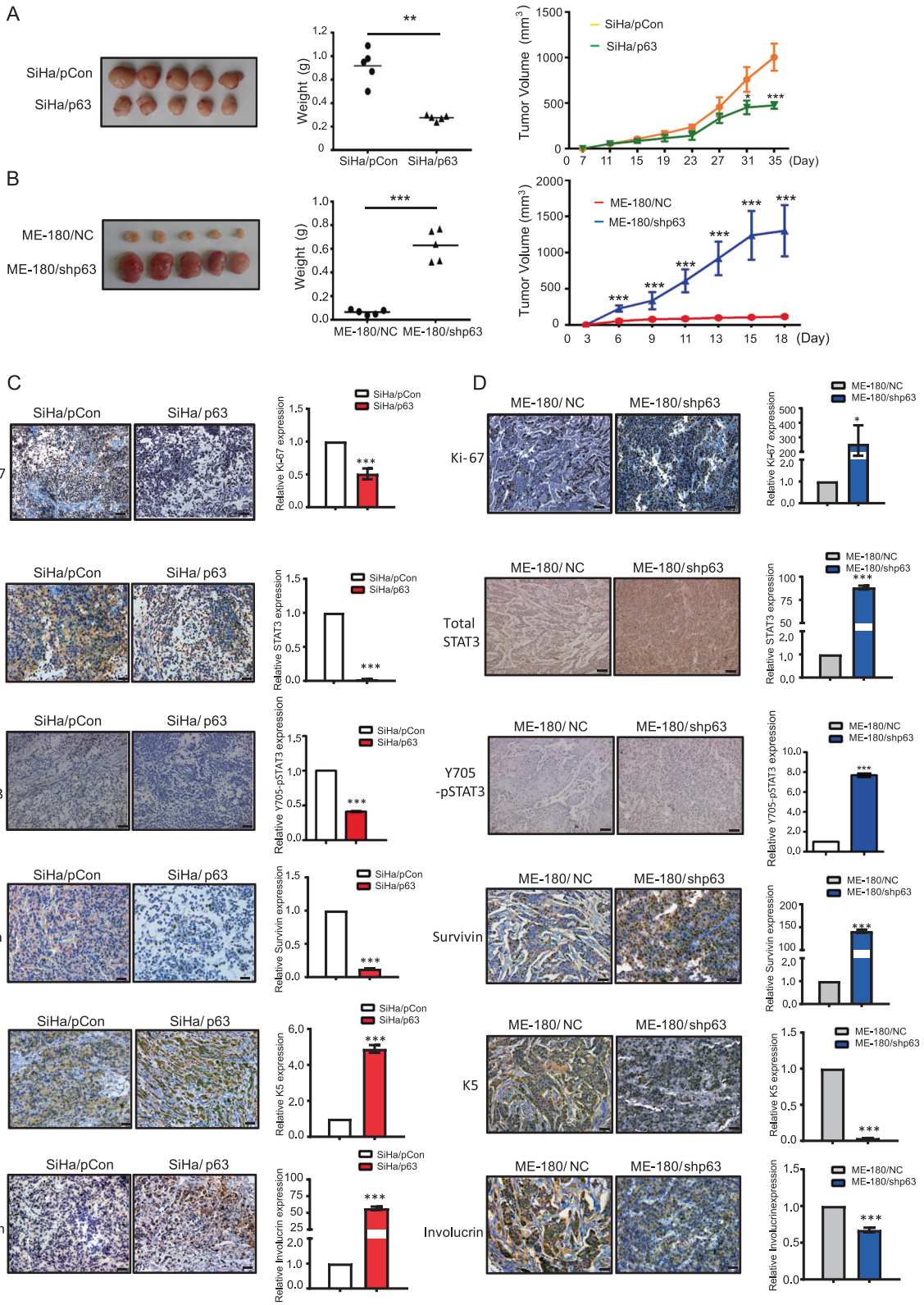

markers and upregulation of mesenchymal markers both in cultured cells and xenograft tumors (Fig. 3c, d). Knockdown of ΔNp63α also seemed to alter the morphology of ME-180 cells; they became smaller, slimmer, and fibroblastic-shaped, and had branched protrusions (Fig. 3e). Tissues from dissected tumors with H&E staining revealed that knockdown of ΔNp63α altered the morphology of ME-180 cells (Fig. 3f).

◀ **Fig. 2** ΔNp63α inhibits proliferation of cervical squamous cells in vivo. **a** Tumors derived from SiHa/p63 and the corresponding control cells. Weights (middle) and volumes (right) of tumors are also shown. $n = 6$ tumors. **b** Tumors derived from ME-180/shp63 and the corresponding control cells. Weights (middle) and volumes (right) of tumors are also shown. $n = 6$ tumors. **c** Representative images of proliferation-related markers (Ki-67, total STAT3, Y705-pSTAT3, and survivin) and differentiation-related markers (K5 and Involucrin) in SiHa/p63-derived tumors (SiHa/pCon as the vector only control) by immunohistochemistry. **d** Representative images of proliferation-related markers (Ki-67, total STAT3, Y705-pSTAT3, and survivin) and differentiation-related markers (K5 and Involucrin) in ME-180/shp63-derived tumors (ME-180/NC as the no-knockdown control) by immunohistochemistry. $*p < 0.05$, $**p < 0.01$, $***p < 0.001$ are based on the Student's *t*-test. Error bars, SD. For **a** and **b**, $n = 5$. For **c** and **d**, $n = 3$. Scale bar: 40 μm

ΔNp63α suppresses the migration and invasion of CSCC as well as the angiogenesis of CSCC-derived tumors

To evaluate the effect of ΔNp63α on cell motility, we performed wound healing assay and transwell assay. SiHa/p63 cells migrated significantly slower compared with the control cells (Fig. 4a). However, ME-180/shp63 cells with ΔNp63α knockdown migrated significantly faster compared with the control cells (Fig. 4b). Moreover, SiHa/p63 cells showed weaker migration and invasion capability in matrigel (Fig. 4c). In addition, ME-180/shp63 cells with ΔNp63α knockdown increased migration and invasion compared with the control cells (Fig. 4d).

The effects of ΔNp63α on angiogenesis of cervical squamous carcinoma cells were then examined. We found that the expression levels of VEGF were significantly lower in SiHa/p63 cells compared with the control, while the expression levels of VEGF were significantly higher in ME-180/shp63 cells compared with their corresponding controls (Fig. 4e). The SiHa/p63-derived tumors expressed a lower number of CD34 positive blood vessels, while the ME-180/shp63-derived tumors expressed a higher number of CD34 positive blood vessels, compared with the corresponding controls (Fig. 4f). The number of blood vessels was 13.1 ± 1.2/mm^2 in SiHa/ΔNp63α group as compared with 35 ± 1.6/mm^2 in the control group; 27 ± 0.63/mm^2 in ME-180/shp63 group as compared with 12 ± 1.57/mm^2 in the control group (Fig. 4f). Thus, higher expression levels of ΔNp63α expression inhibit cell migration and invasion in CSCC, and angiogenesis of CSCC-derived tumors.

Identification of target genes of ΔNp63α in cervical squamous cancer cells

To better understand the transcriptional regulatory mechanisms of ΔNp63α in cervical squamous carcinoma cells, we performed RNA-seq in ME-180/shp63 and SiHa/p63 cells, respectively (Fig. 5a). In ME-180/shp63 RNA-seq, mRNAs of 6263 genes were significantly affected (cutoff of twofold changes and $p < 10^{-5}$) compared with the no-knockdown control (Fig. 5a and Supplementary Fig. S3A). In SiHa/p63 RNA-seq, 230 genes were significantly affected (cutoff of twofold changes and $p < 10^{-5}$) compared with the no-overexpression control (Fig. 5a and Supplementary Fig. S3B). Thus, cervical squamous carcinoma cells might be more sensitive to decreased levels of ΔNp63α. There were 100 overlapped genes (with reversed changes, since the experimental cells were with knockdown and overexpression of ΔNp63α, respectively) from these two RNA-seq data (Fig. 5a, b). These genes could be either direct or indirect targets of ΔNp63α. GO analyses of these 100 genes revealed enrichment in terms such as keratinization, cornification, signal transduction, programmed cell death, and cell differentiation (Fig. 5c).

To determine global direct targets of ΔNp63α, we performed ChIP-seq of endogenous p63 in ME-180 cells. Bioinformatics analysis of the ChIP-seq data identified 3349 p63 direct target genes (Fig. 5d). Among the 100 genes significantly affected by ΔNp63α in the RNA-seq analyses, 33 possessed p63 ChIP-seq binding sites, and thus should be direct targets of ΔNp63α (Fig. 5d). We also analyzed the distribution of p63 ChIP-seq peaks relative to the genomic region (Fig. 5e). p63 ChIP-seq signals formed a major peak around 0.2 kb downstream of the transcription start sites (TSS) (Fig. 5f); this feature of p63 ChIP-seq peak is also seen in other types of tumor [30–33]. De novo analysis showed that the p63-binding motif in cervical squamous carcinoma cells matched the p63-binding site of "CNNG" found in other cell types (Fig. 5g) [30, 33]. These 33 genes were direct ΔNp63α targets and substantially regulated in both CSCC cell lines. These direct targets could be either activated or suppressed by ΔNp63α (Fig. 5h and Supplementary Fig. S4). GO analyses of these 33 genes revealed enrichment in four terms all related to cell junctions (Fig. 5i).

We then examined all the 33 candidate genes with survival curves in two online databases, Kaplan–Meier Plotter (KMP) and Xena Functional Genomics Explorer (XFGE). XFGE database (http://xenabrowser.net) includes data from cervical cancer, which includes both CSCC and cervical adenocarcinoma. Therefore, we could not specifically analyze CSCC, and two genes CLDN1 and ZNF385B were correlated to survival curves of cervical cancers (Fig. 5j). In KMP database (http://kmplot.com/analysis), data from CSCC are collected, and this database does not have data from cervical adenocarcinoma. 12 out of the 33 genes were correlated to survival curves of CSCC in KMP (Supplementary Fig. S5). CLDN1 and ZNF385B are in these 12

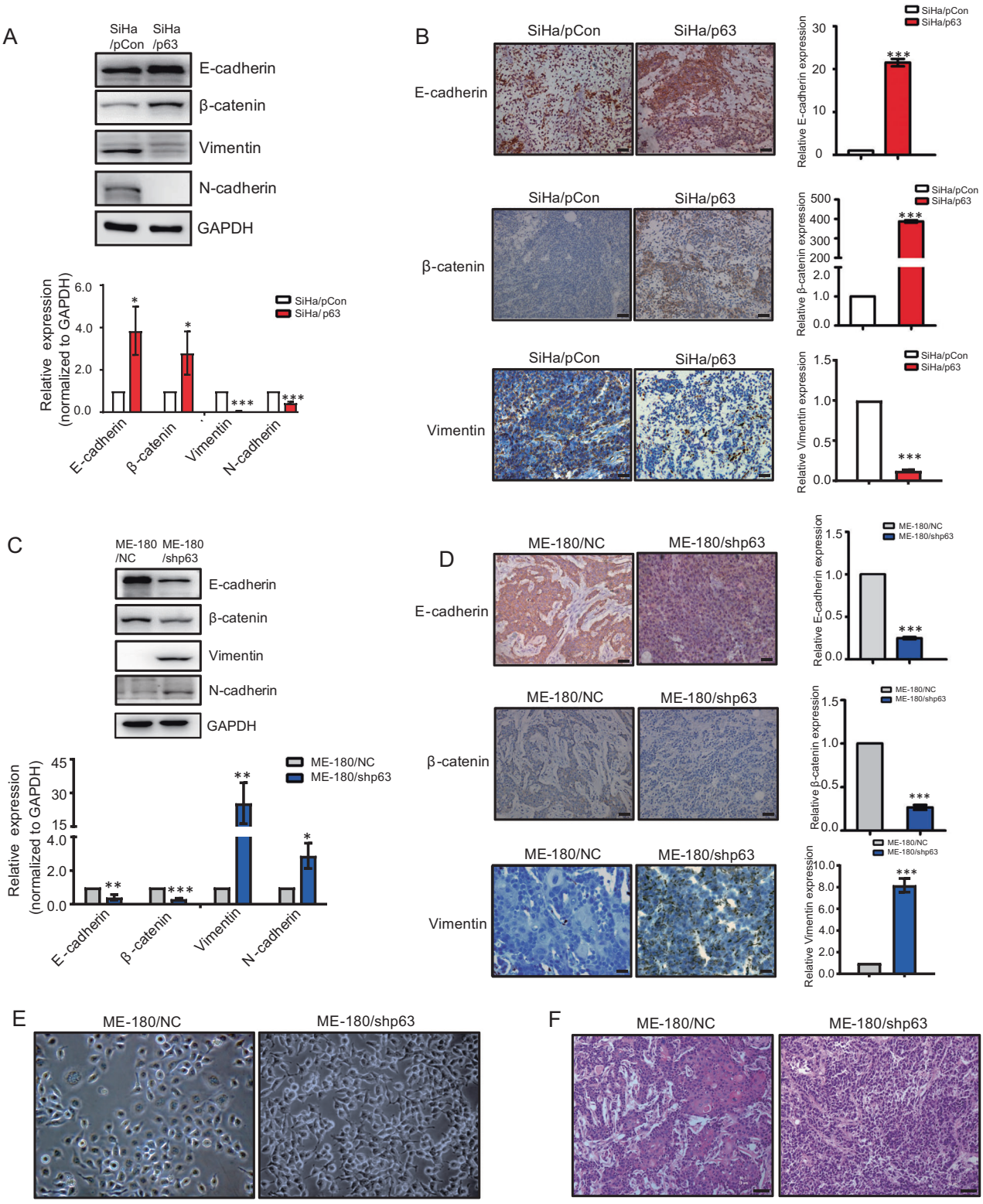

genes. We hence focused on CLDN1 and ZNF385B for downstream examination. ChIP-seq peaks for both genes and ChIP efficiency were shown (Supplementary Fig. S6A, B). Interestingly, the correlation with survival for the expression levels of CLDN1 is positive, while that of ZNF385B is negative (Fig. 5j and Supplementary Fig. S5). In accordance with this, the expression of CLDN1 was activated by ΔNp63α, and the expression of ZNF385B was

◀ **Fig. 3** ΔNp63α regulates epithelial–mesenchymal transition in cervical squamous carcinoma cells. **a** Expression of epithelial (E-cadherin and β-catenin) and mesenchymal (Vimentin and N-cadherin) markers were analyzed by western blot in SiHa/p63 and the control. **b** Representative images of E-cadherin, β-catenin, and Vimentin expression in SiHa/p63 cells xenograft tumors by immunohistochemistry. **c** Expression of epithelial (E-cadherin and β-catenin) and mesenchymal (Vimentin and N-cadherin) markers are analyzed by western blot in ME-180/shp63 and the control. **d** Representative images of E-cadherin, β-catenin, and Vimentin expression in ME-180/shp63-derived tumors by immunohistochemistry. **e** Comparison of morphology between cultured ME-180/shp63 and the control cells. **f** Cell morphology in tissue section slides between ME-180/shp63 and the control by H&E staining. All the experiments were performed in triplicates. Error bars, SD, data are means ± SEM. n.s., not significant, $*p < 0.05$, $**p < 0.01$, $***p < 0.001$, are based on the Student's *t*-test. Scale bar: 40 μm

suppressed by ΔNp63α in CSCC cell lines (Fig. 5h and Supplementary Fig. S4).

ΔNp63α regulates CLDN1 and ZNF385B in cultured cells and clinical samples

We examined the expressions of CLDN1 and ΔNp63α in CSCC cells and clinical samples. Both SiHa/p63 cells and SiHa/p63-derived tumors showed significantly increased levels of CLDN1 protein (Fig. 6a, b). On the other hand, ME-180/shp63 cells, and ME-180/shp63-derived tumors showed significantly decreased levels of CLDN1 (Fig. 6a, b). Expression of ΔNp63α and CLDN1 was also significantly decreased in the cervical tumor samples, compared with adjacent normal tissues (Fig. 6c). Pearson correlation coefficient analyses showed that ΔNp63α expression was positively associated with CLDN1 in clinical tissues ($r = 0.6025$ and $P < 10^{-4}$) (Fig. 6d). As for ZNF385B, SiHa/p63 cells, and SiHa/p63-derived tumors showed decreased levels of ZNF385B compared with their corresponding controls; ME-180/shp63 cells and ME-180/shp63-derived tumors showed significantly increased levels of ZNF385B (Fig. 6e, f). ZNF385B expression was also significantly increased in the cervical tumor samples, compared with adjacent normal tissues (Fig. 6g). Pearson correlation coefficient analyses revealed that the ΔNp63α expression was inversely associated with ZNF385B expression in clinical tissues ($r = -0.4831$ and $P = 0.0008$) (Fig. 6h). As we showed that ΔNp63α affected the EMT behavior in CSCC (Fig. 3a–d), we also examined the involvement of CLDN1 and ZNF385B in EMT in SiHa and ME-180 cells through examining expression of epithelial and mesenchymal markers by Western blot. Overexpression of CLDN1 in SiHa significantly increased EMT, whereas knockdown of CLDN1 in ME-180 decreased EMT significantly. On the other hand, knockdown of ZNF385B in SiHa significantly increased EMT, while the overexpression of ZNF385B in ME-180 decreased EMT (Supplementary Fig. S7).

ΔNp63α downregulates NFATC1 to reduce cisplatin resistance in cervical squamous cancer cells

Several recent studies indicated that one of the 33 direct targets of ΔNp63α, NFATC1, might play roles in cisplatin resistance in several types of tumors other than CSCC [34–36] (Supplementary Fig. S4). ChIP-seq peaks for NFATC1 and ChIP efficiency were shown (Supplementary Fig. S6C, D). Apoptosis of SiHa/p63 and ME-180/shp63 cells under treatment with cisplatin was then examined, and we found that apoptosis of SiHa/p63 increased significantly after the overexpression of ΔNp63α, while ME-180 decreased significantly after the knockdown of ΔNp63α (Fig. 7a–d). Furthermore, ΔNp63α overexpression decreased the levels of NFATC1 in SiHa/p63 cells, and ΔNp63α knockdown significantly increased the levels of NFATC1 (Fig. 7e). NFATC1 expression was significantly increased in cervical cancer samples, compared with adjacent normal tissues (Fig. 7f). Expression levels of ΔNp63α were inversely associated with NFATC1 expression in clinical serial sections ($r = -0.3012$ and $P = 0.0444$) (Fig. 7g). The proliferation of ME-180/shp63 cells decreased significantly upon silencing NFATC1 when treated with cisplatin (Fig. 7h). Cell apoptosis also increased significantly after inhibiting NFACT1 in cisplatin-treated ME-180/shp63 (Fig. 7i and Supplementary Fig. S8).

Discussion

In this study, we have unveiled the antitumor roles of ΔNp63α in CSCC. We have demonstrated these roles with several layers of evidence. By knocking down or overexpressing ΔNp63α, we have found that ΔNp63α reduced cell proliferation, inhibited epithelial–mesenchymal transition, and suppressed migration and invasion of CSCC both in cell cultures and in tumor xenografts. ΔNp63α indeed plays tumor-specific roles to be either a tumor gene or a tumor suppressor in distinct types of cancers [20–22].

We have identified a small group of genes by RNA-seq and ChIP-seq as the core of ΔNp63α targets. It is interesting that 6263 genes were significantly affected in ME-180/shp63 based on RNA-seq data, but only 230 genes were significantly affected in SiHa/p63 RNA-seq (Fig. 5a). The distinct gene regulatory network that associates with p63 in ME-180 and SiHa cells maybe distinct to react to changes in the expression levels of ΔNp63α, which we do not fully understand. Another fact maybe related is that the ME-180/shp63 cells had ~20% of p63 protein levels left, and on the other hand, SiHa/p63 overexpressing cells had only ~2

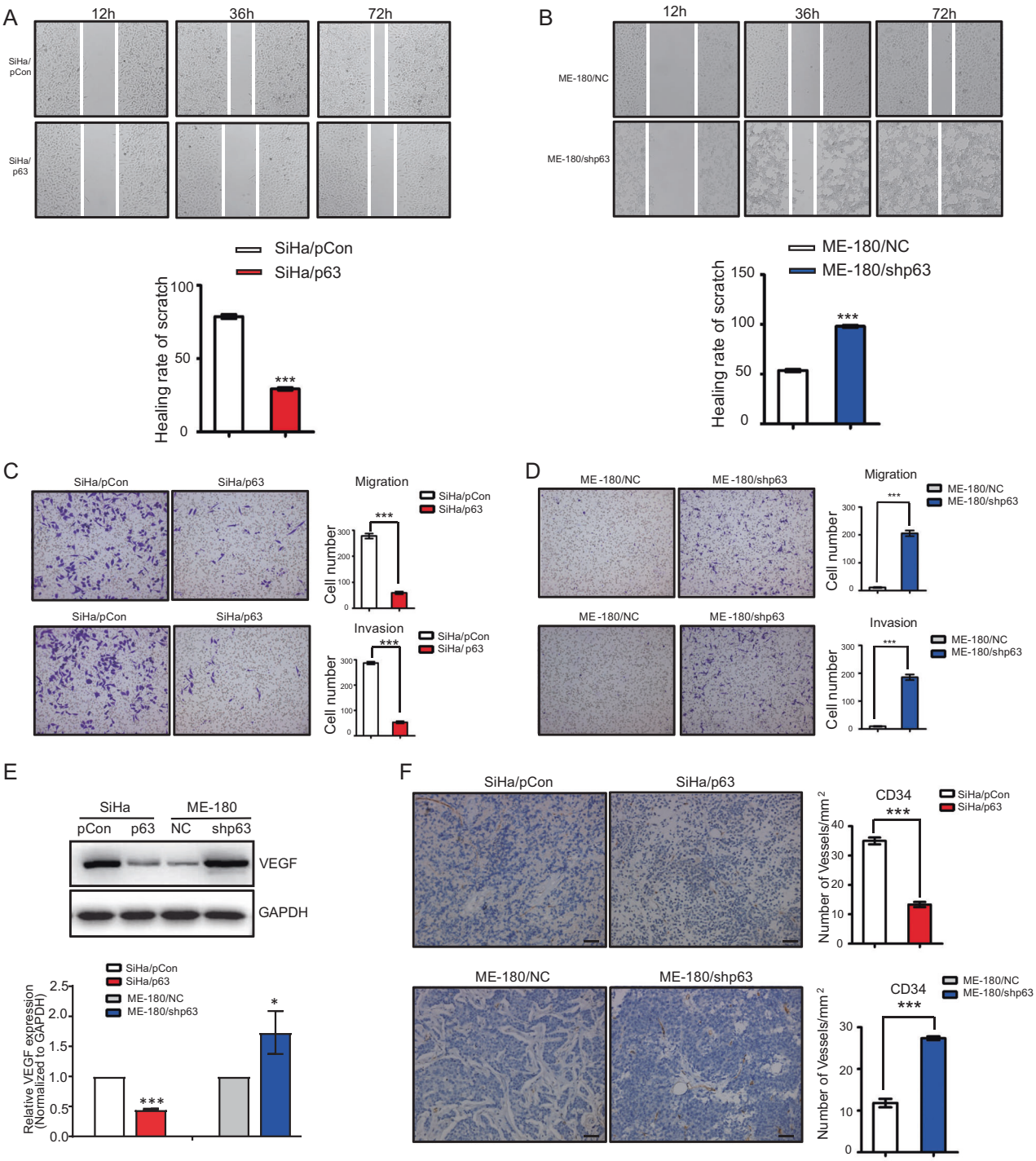

Fig. 4 ΔNp63α suppresses migration, invasion, and angiogenesis of cervical squamous cancerous cells. **a** Representative images of wound healing in SiHa/p63 cells and the control. Quantification of healing rate is also shown. **b** Representative images of wound healing in ME-180/shp63 cells and the control. Quantification of healing rate is also shown. **c** Representative images of transwell migration (top) and Matrigel invasion assays (bottom) of SiHa/p63 cells and the control. Quantification of migrating cells is also shown. **d** Representative images showing transwell migration (top) and Matrigel invasion assays (bottom) of ME-180/shp63 cells and the control. Quantification of migrating cells is shown. **e** Expression of VEGF analyzed by western blot, and the quantification is shown below. **f** CD34 expression in SiHa/p63-derived (upper) and ME-180/shp63-derived (lower) xenograft tumors by immunohistochemistry. Multiple regions ($n = 5$) from different tumors ($n = 6$) are quantified. $^{**}p < 0.01$, $^{***}p < 0.001$, the Student's t-test. In **b**, **c**, and **d**, data are means ± SEM. Error bars, SD. Scale bar: 40 μm

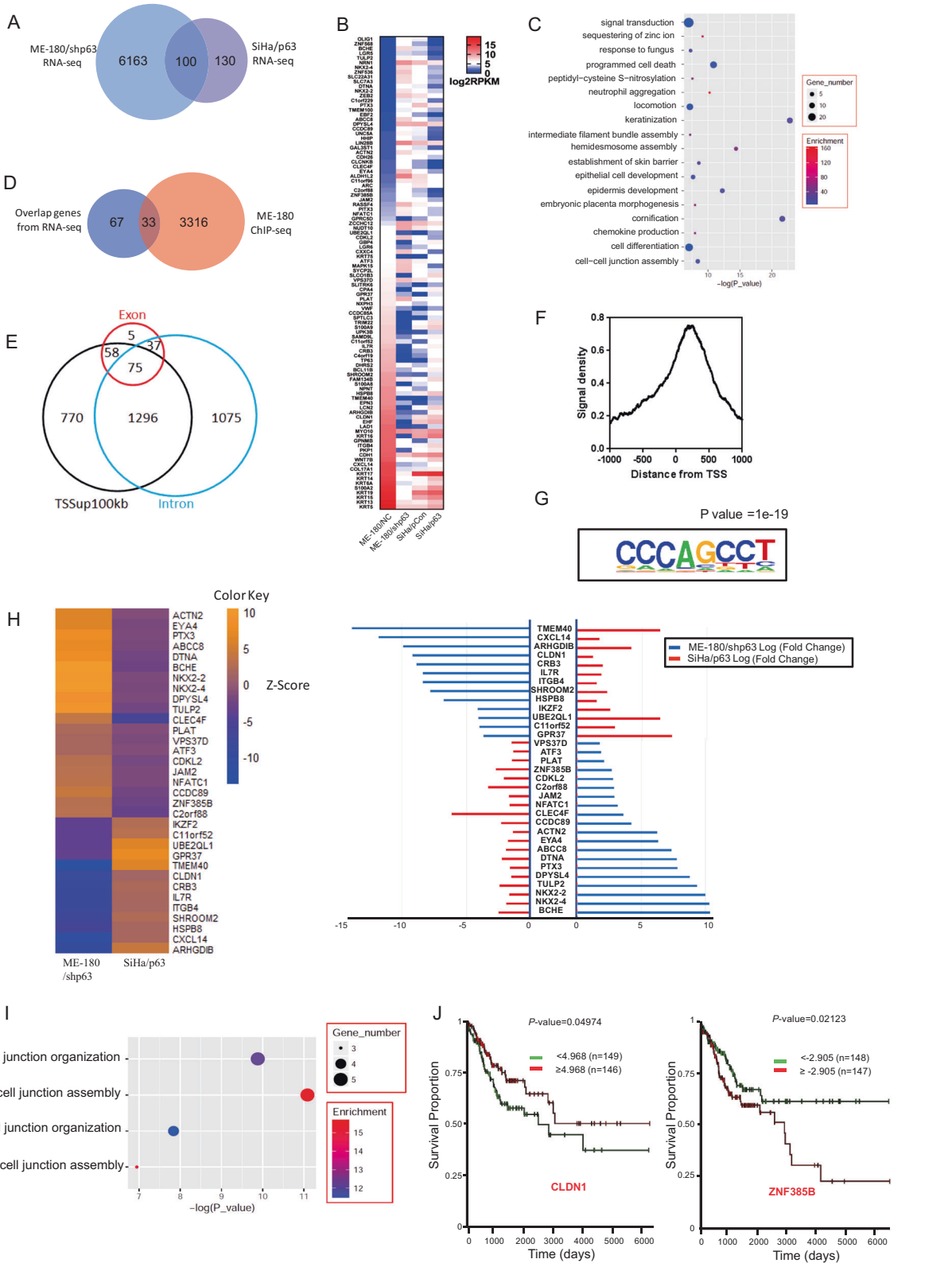

times of p63 protein levels than SiHa control cells (Fig. 1b). The p63 mRNA levels showed much more dramatic changes than p63 protein levels in the overexpression or knockdown (Fig. 1b), suggesting a strong posttranscriptional regulation on p63 expression. The 33 genes are all direct ΔNp63α targets in both cell types, and their expression levels are relatively more sensitive to changes of the ΔNp63α expression to either higher or lower

◀ **Fig. 5** Identification of target genes regulated by ΔNp63α in cervical squamous cancer cells. **a** Analyses of ME-180/shp63 RNA-seq and SiHa/p63 RNA-seq; overlapped genes are shown. **b** The heatmap of the 100 overlapped genes significantly regulated by ΔNp63α in both ME-180 and SiHa cells. **c** GO analyses of biological process for 100 overlapped genes significantly regulated by ΔNp63α in both ME-180 and SiHa cells. **d** Overlapped genes from p63 ChIP-seq and the 100 genes commonly regulated by p63 in both SiHa and ME-180 cells (shown in **a**). **e** Genomic distribution of p63ChIP-seq peaks in the corresponding numbers of genes; TSS transcriptional start site. **g** Distribution of p63 ChIP-seq signals around 1 kb of the TSS. **g**, The most enriched p63-binding motif in ME-180 ChIP-seq data by HOMER (top 100 peaks). **h** Heatmap of RNA-seq data for the 33 ΔNp63α direct targets that are also significantly affected by the overexpression or knockdown of ΔNp63α in SiHa or ME-180 cells, respectively. Quantification of mRNA levels of the 33 targets of ΔNp63α is shown to the right; FC fold change. **i** GO analyses of biological process for 33 overlapped genes from p63 ChIP-seq data and RNA-seq data (shown in **h**). **j** Survival curves of CLDN1 and ZNF385B analyzed by Xena Functional Genomics Explorer; *p* value was calculated by log-rank test

levels (Fig. 5d). This core of genes enriches for functions in cell junction. It is well established that cell junctions play essential roles in epithelial cells, and they are well known to be related to multiple aspects of tumors and regulate cell proliferation, epithelial–mesenchymal transition, metastasis, and angiogenesis [37–40]. One of the two core target genes of ΔNp63α with significant association with patient survival, CLDN1, is an intercellular junction gene [41]. CLDN1 was previously reported to be involved in cell migration and metastasis, and its expression was also related to lung cancer, gastric cancer, colorectal cancer, and triple-negative breast cancer [42–45]. Notably, Phospho-ΔNp63α was shown to upregulate miR-185-5p and downregulate let7-5p to regulate CLDN1 through its 3′-UTR [46]. Also, CLDN1 was found to be involved in epithelial development regulated by ΔNp63α [47]. Another core target of ΔNp63α is NFATC1, a well-studied nuclear factor that is regulated by multiple signaling pathways and has critical roles in the differentiation of osteoclast [34, 35]. NFATC1 is also a major clinical target for immunosuppressive drugs [36, 48]. Detailed molecular mechanism about how NFATC1 is related to cisplatin resistance remains for further investigation. Molecular functions of the other ΔNp63α core target gene with significant association with patient survival, ZNF385B, are largely unknown.

p53 is an important tumor suppressor, and its structural homologs p63 and p73 can have both similar and distinct functions from p53 [49]. Actually, more than 40 different isoforms of the p53 family members via transcription from different promoters or alternative splicing are currently known [49]. p53 family genes can be used for cancer prognosis and furthermore as potential targets for cancer therapy [50], and thus it is of great importance to evaluate roles of isoforms such as ΔNp63α in various tumors. Different from p53, the presence of a Sterile Alpha Motif (SAM) renders p63 the most significant structural difference [51]. SAM domains are protein–protein interaction domains also found in other developmentally important proteins, such as p73 and several Eph receptor tyrosine kinases [52]. ΔNp63α is the predominant isotype expressed in the cervix, playing the fundamental role in the regulation of cervical squamous tumorigenesis. As a transcription factor, ΔNp63α can both activate the expression of target genes (e.g., CLDN1) and inhibit the expression of some other target genes (e.g., ZNF385B and NFATC1) as demonstrated in this study, maybe due to the combinatory effects of transcriptional regulators. Our study demonstrates that at least in CSCC cell lines examined and in the contexts of our experimental setup, ΔNp63α has antitumor effects by regulating specific target genes. The characterization of ΔNp63α as an important regulator in CSCC and further the identification of ΔNp63α core targets such as cell junction genes, CLDN1, ZNF385B, and NFATC1 are potentially with fundamental significance in the understanding, prognosis, and treatment of CSCC.

Materials and Methods

Cell culture

SiHa and ME-180 cells (ATCC, Manassas, VA, USA) were maintained in Dulbecco's modified eagle medium (DMEM) (Hyclone, Logan, UT, USA) or McCoy's 5 A Medium (Gibco) with 10% (v/v) fetal bovine serum (Gibco, Thermo Fisher Scientific, Waltham, MA, USA) respectively, containing 100 units/ml penicillin and 100 mg/ml streptomycin (Hyclone). Both SiHa and ME-180 cells were tested for mycoplasma by a PCR-based method as well as DAPI staining, to ensure the absence of contamination. We did this test routinely once every 2 months or at the beginning of the new series of experiments. Both cell lines are not in the database of commonly misidentified cell lines that is maintained by ICLAC (most recent version, Version 8.0) and NCBI Biosample.

Plasmids construction

Human ΔNp63α cDNA was cloned by RT-PCR. ΔNp63α cDNA was inserted into MIGR1-Puro (Addgene, #27490). The ΔNp63α target shRNA sequences (ACAGACCC TTTGTAGCGTG, at position 3648 to 3666) were achieved from School of Life Sciences, University of Science and Technology of China. After screening with transient transfection with shRNAs, the synthetic antisense oligonucleotides and a shRNA control were cloned into pLKO.1 puro vector.

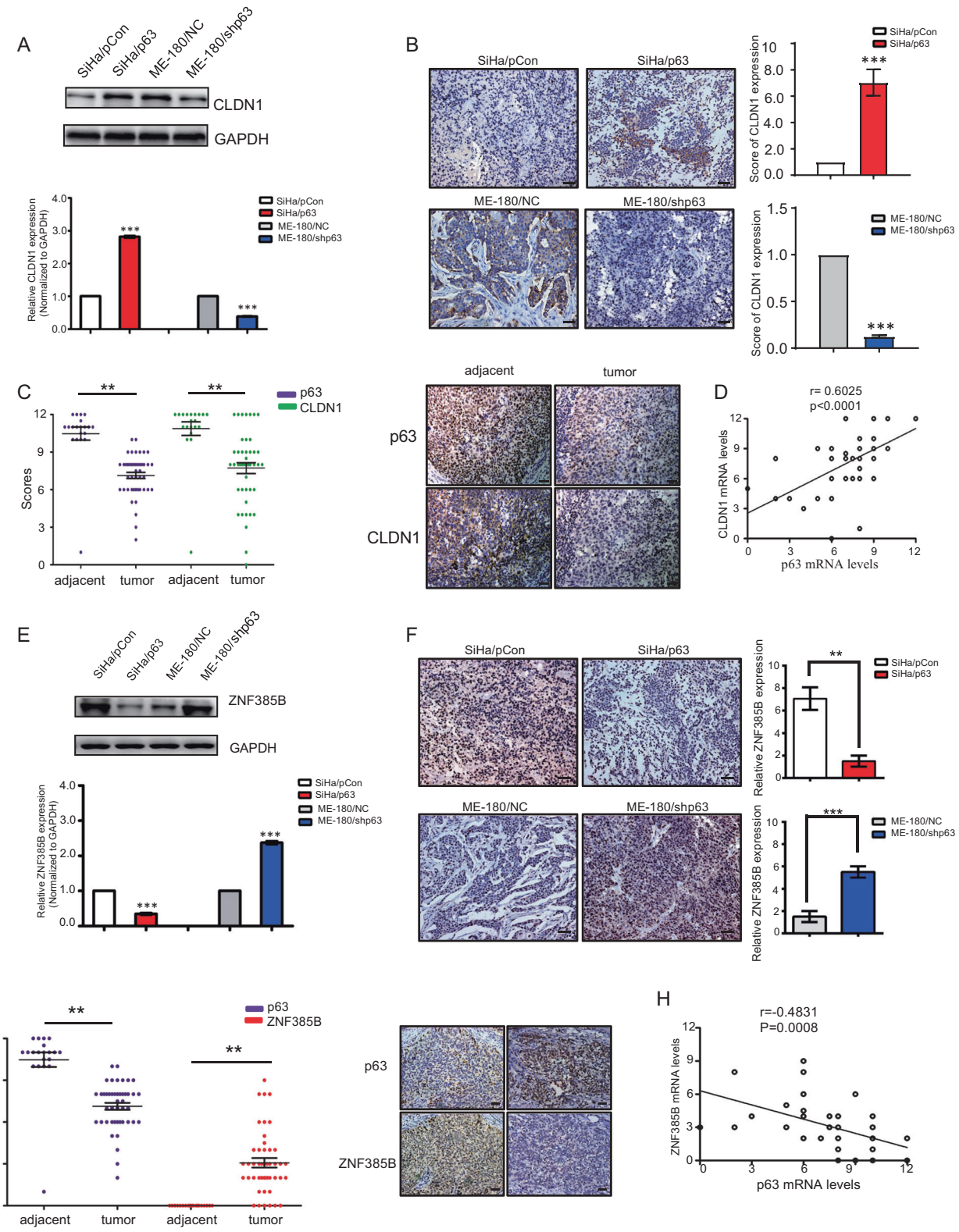

Stable cell lines

To construct SiHa/p63 stable cell line, MIGR1-ΔNp63α plasmid and pCL-10A1 packaging vector were co-transfected into 293T cells. Then the virus supernatant infected SiHa cells, respectively. SiHa/p63 stable cell lines and SiHa/pCon cells were generated by selection with 2 μg/ml puromycin (Merck) for 2 weeks as described previously [53]. To

◀ **Fig. 6** Correlations of ΔNp63α with CLDN1 and ZNF385B in their gene expression. **a** Western blot of CLDN1 in SiHa/p63, ME-180/shp63, and the corresponding control cells. **b** Representative images of CLDN1 expression in SiHa/p63-derived (upper) and ME-180/shp63-derived (lower) xenograft tumors by immunohistochemistry are shown. Quantifications were on the right. **c** Scatterplot of CLDN1 staining scores in the tumor ($n = 45$) and adjacent cervix tissues is shown ($n = 20$). Representative images of ΔNp63α and CLDN1 in clinical tissues of cervical cancer by immunohistochemistry are shown (right). **d** Correlation between the expression of ΔNp63α and CLDN1 in cervical cancer tissues. $n = 45$. **e** Western blot for ZNF385B in SiHa/p63, ME-180/shp63 cells, and their respective controls. **f** Representative images showing ZNF385B expression in SiHa/p63-derived and ME-180/shp63-derived xenograft tumors by immunohistochemistry. Quantifications were also shown. **g** Scatterplot of ZNF385B staining scores in the tumor ($n = 45$) and adjacent cervix tissues ($n = 20$). Data of ΔNp63α (labeled as p63) are the same as used in **c**. Representative images of ΔNp63α and ZNF385B in clinical tissues of cervical cancer by immunohistochemistry are shown (right). **h** Correlation between the expression of ΔNp63α and ZNF385B in cervical cancer tissues. In **a**, **b**, **c**, **e**, **f**, and **g**, data are means ± SEM. $^{**}p < 0.01$, $^{***}p < 0.001$ are based on the Student's *t*-test. Error bars, SD. For **d**, $r = 0.6025$; $p < 0.0001$, and for **h**, $r = -0.4831$; $p = 0.0008$. For tumor experiments, $n = 6$ pairs. Scale bar: 40 μm

construct ME-180/shp63 stable cell line, ME-180 cells were transfected with recombinant lentiviruses pLKO-puro harboring sh-NC, sh-ΔNp63α named ME-180/NC and ME-180/shp63 respectively, and the stable cell lines were also treated and screened with 2 μg/ml puromycin for 2 weeks.

Quantitative real-time PCR

Total RNA was isolated from cells or tissues by TRIzol reagent (Invitrogen) according to the manufacturer's protocol. Reverse transcription was performed by PrimeScript TM RT Reagent Kit (Invitrogen) following the protocol, then qRT-PCR was carried out in a final volume of 20 μl containing 1 μl of cDNA, 1 μl primers (10 μM), 10 μl SYBR Green PCR Master Mix (Roche) in real-time PCR instrument (Thermo). 18S rRNA and GAPDH were served as controls. All the primers for detection were shown in Supplementary Table S1.

Immunoprecipitation and immunoblotting analysis

Immunoprecipitation and immunoblotting analysis were performed as described previously [54, 55]. Briefly, cell lysates were incubated with the appropriate primary antibodies or normal mouse IgG for 2 h at 4 °C followed by the addition of Protein G-agarose beads for 2 h at 4 °C. The bound complexes were then washed three times with RIPA buffer and were eluted in SDS sample loading buffer. The eluted proteins or total extracted proteins were separated by SDS-PAGE and transferred to polyvinylidene fluoride membrane (Millipore, Billerica, MA, USA), and detected with specific primary antibodies coupled with horseradish peroxidase-conjugated secondary antibody by the enhanced chemiluminescence detection reagent (GE healthcare Life Sciences, Piscataway, NJ, USA). The antibodies were also shown in Supplementary Table S1.

Chromatin immunoprecipitation (ChIP)

ChIP assay and ChIP qRT-PCR were performed as described previously [54, 55]. Briefly, Cells were cross-linked in a UV cross-linker (UVP) at 200 mJ. After rinsed with phosphate buffer saline (PBS) twice, cell pellets were lysed in 1 ml of SDS lysis buffer (1% (w/v) SDS, 10 mM EDTA, and 50 mM Tris-HCl, pH 8.1) containing complete protease inhibitor cocktail (Roche) and were incubated for 20 min on ice. Cell extracts were sonicated for 5 min with a Sonics Vibra-Cell. A 100 μl sample of the supernatant was saved as input. The remaining sample was diluted in 1:10 in ChIP dilution buffer (0.01% (w/v) SDS, 1.1% (v/v) Triton X-100, 1.2 mM EDTA, 16.7 mM Tris-HCl, pH 8.1, and 167 mM NaCl) containing protease inhibitors. The chromatin solution was precleared and immunoprecipitated with 2 μg of p63 antibody or normal IgG control. The immunocomplexes were eluted in 1% (w/v) SDS and 50 mM $NaHCO_3$, and cross-links were reversed for 6 h at 65 °C. Samples were digested with proteinase K for 1 h at 45 °C, and the DNA was extracted with phenol/chloroform/isoamyl alcohol. Eluted DNA was subjected to quantitative real-time PCR detecting enriched genomic DNA regions with the corresponding primers. The antibodies and primers were also shown in Supplementary Table S1.

mRNA library preparation and sequencing

mRNA-seq was performed as described previously [55]. Overall 5 μg of RNA treated with siRNA or plasmid was heated at 95 °C and then subjected to end repair and 5′-adaptor ligations. Reverse transcription was carried out with random primers containing 3′ adaptor sequences and randomized hexamers. The cDNAs were purified and amplified, and PCR products of 200–500 bp were purified, quantified and stored at −80 °C until sequencing. For high-throughput sequencing, the libraries were prepared according to the manufacturer's instructions and subjected to 151-nt paired-end sequencing with an Illumina Nextseq 500 system. We sequenced each library to a depth of 10–50 million read pairs. To obtain clean reads, adapters were removed with cut adapt.

ChIP-Seq data analysis

For ChIP-seq data analysis, we filtered out reads from the genomic repeats, then the unique reads were mapped to the human genome (hg19) with bowtie (-v1). Peaks of p63 were

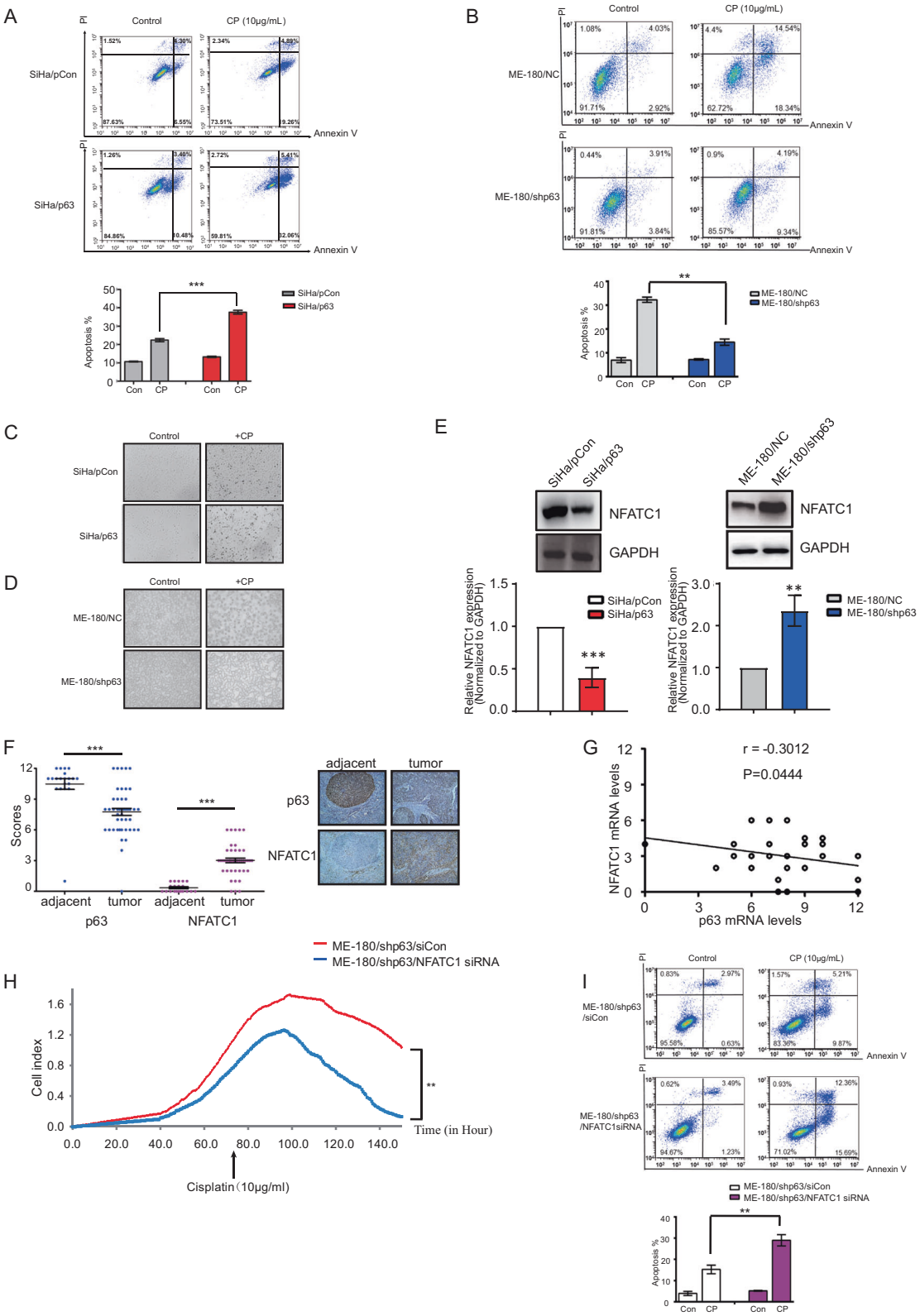

found with cisGenome, by comparing ChIP to the corresponding input (cutoff >twofolds and p value $< 10^{-5}$), and genes were generated with peaks distances of 10 kb from the TSSs. The enriched motif of p63 was generated by HOMER with the top 100 peaks. All peak signals were shown with IGV. The p values generated in the analysis of

◀ **Fig. 7** ΔNp63α downregulates NFATC1 to reduce cisplatin resistance in cervical squamous cancer cells. **a** Flow cytometry analysis of apoptosis induced by cisplatin (CP) in SiHa/p63 and its control cells. Quantitative analysis of apoptotic cells is shown. **b** Flow cytometry analysis of apoptosis induced by cisplatin (CP) in ME-180/shp63 and its control cells. Quantitative analysis of apoptotic cells is shown. **c** Representative images of cell apoptosis in SiHa/p63 and its control treated with/ without cisplatin (CP). **d** Representative images of cell apoptosis in ME-180/shp63 and its control treated with/without cisplatin (CP). **e** Western blot for NFATC1 in SiHa/p63, ME-180/shp63, and the respective controls. Quantitative analysis is shown. **f** Scatterplot of NFATC1 staining scores in the tumor ($n = 45$) and adjacent cervix tissues ($n = 20$). Data of ΔNp63α (labeled as p63) are the same as used in Fig. 6c, g. Representative images of ΔNp63α and NFATC1 in clinical tissues of cervical cancer by immunohistochemistry (right). **g** Correlation of the expression levels between ΔNp63α and NFATC1 in cervical cancer tissues ($n = 45$)**. h** Proliferation of ME-180/shp63 cells treated with/without cisplatin after NFATC1 knockdown determined by ACEA; time points of cisplatin treatment are indicated. **i** Flow cytometry analyses of apoptosis induced by cisplatin after the knockdown of NFATC1. Quantification of apoptotic cells is shown (lower). $^{**}p < 0.01$, $^{***}p < 0.001$ are based on the Student's *t*-test. In **a**, **b**, **e**, **h,** and **i**, data are means ± SEM in triplicates. Error bars, SD. For **e**, $r = -0.3012$; $p = 0.0444$. Scale bar: 40 μm

ChIP-seq data were calculated by default parameters of the respective software.

Cell proliferation in vitro (ACEA)

A total of 6×10^4 cells (including SiHa/pCon, SiHa/p63 and ME-180/NC, ME-180/shp63 cells, respectively) were resuspended in 1 ml DMEM containing 10% FBS. A total of 100 μl of the cell suspension were seeded into each well of the ACEA 16-well plate and put into the xCELLigence RTCA DP measuring instrument (Roche). The number of cells per well was then counted at the indicated time points. Each type of cells was counted in triplicates. The cell growth plot was analyzed by xCELLigence (ACEA Biosciences Inc.).

Colony formation assay

The number of all cells per well was counted and cells were kept uniform distribution. For SiHa/pCon and SiHa/p63 cells, 100 and 300 cells were split into six-well plates separately and in triplicates. Cells were allowed to grow for 14 days in 5% CO_2 incubators before being stained with 0.5% Crystal Violet Staining Solution (Solarbio). For ME-180/NC, ME-180/shp63 cells, 100, and 200 cells were split into six-well plates separately and in triplicates. Cells were allowed to grow for 10 days in 5% CO_2 incubators before stained with 0.5% Crystal Violet Staining Solution.

Cell cycle detection

A total of 2×10^5 cells were plated in six-well plates per well and cultured overnight. Then all cells were starved in serum-free medium for 48 h. Cells were then changed with complete medium for another 24 h. The cells in each group were fixed with 70% ethanol overnight and washed with PBS twice. According to the protocol of Cell Cycle Detection Kit (Beyotime, China), the cells were resuspended with 400 μl of binding buffer and stained with 20 μl of propidium iodide (PI) for 20 min at room temperature in darkness. Cell cycle was analyzed immediately with flow cytometry (Becton-Dickinso, FACSCalibur). The percentage of cells at each phase of cell cycle was obtained by Cell Quest software (Becton-Dickinso, FACSCalibur).

Scratch, migration, and invasion assays

For scratch assays, 400,000 cells (including SiHa/pCon, SiHa/p63, ME-180/NC, and ME-180/shp63, respectively) were plated in six-well plates, respectively. After the cells were attached, cell monolayers were scraped by a 200 μl pipette tip and washed by PBS to remove cell debris gently. All cells were cultured in 1% FBS in DMEM or McCoy's 5 A medium. Photos were taken during the subsequent 12 h, 36 h, and 72 h. For transwell migration assay, cell suspension containing 4×10^5/ml cells in serum-free media were prepared, followed by addition of 1 ml of media containing 10% fetal bovine serum to the lower chamber. 500 μl of prepared cell suspension was added from each insert (Millipore# PIEP30R48, pore size: 8 μm). For transwell invasion assay, add 300 μl of warm serum-free media to the interior of the inserts and allow this to rehydrate the ECM layer for 1 h at room temperature. A total of 2×10^4 cells were plated into transwell inserts (Chenicon, pore size: 8 μm). All the steps were strictly followed by the transwell migration and invasion assay kit protocols. After 24 h, cells that did not migrate were removed by scratching the upper side of the membrane with a cotton swab before fixation in 4% methanol for 5 min at room temperature. Cells were then stained with Hoechst reagent for 5 min. The percentage of migration was quantified by ImageJ.

Flow cytometric cell death assay

A total of 5×10^5 cells were plated each well of six-well plates and cultured overnight. The cells were grown up to 70% confluency and treated with various drug concentrations of cisplatin for 48 h. Total cells were collected and washed twice in binding buffer and stained with allophycocyanin labeled annexin-V (BioLegend) and PI as per the manufacturer's guidelines. The population was then

analyzed for the percentage of cells in normal, early apoptotic and late apoptotic phase using CytExpert software.

Immunohistochemistry

Formalin-fixed paraffin-embedded 2 μm tissue sections were deparaffinized in xylenes and rehydrated through a graded series of alcohols. After antigen retrieval was performed, all sections were blocked at room temperature in 3% hydrogen peroxide for 10 min. Staining with antibodies was conducted at room temperature for 2 h. Sections were rinsed twice in PBS, and protein staining was performed using diaminobenzidine substrate kit. Samples were counter-stained with hematoxylin. Immunohistochemistry images were obtained using an upright microscope (Olympus). Brown staining indicated the immunoreactivity of samples.

Immunoreactivity was semiquantitatively evaluated based on staining intensity and distribution using the immunoreactive score: immunoreactive score = intensity score × proportion score. The intensity score was defined as 0, negative; 1, weak; 2, moderate; or 3, strong, and the proportion score was defined as 0, negative; 1, <10%; 2, 11~50%; 3, 51~80%; or 4, >80% positive cells. The total score ranged from 0 to 12. The immunoreactivity was divided to three levels on the basis of the final score: negative immunoreactivity was defined as a total score of 0, low immunoreactivity was defined as a total score of 1~4, and high immunoreactivity was defined as a total score >4. The stained tumor tissues were scored by two researchers blinded to the clinical patient data. Quantification was performed using Image-Pro plus 6.0 software. The antibodies were also shown in Supplementary Table S1.

Tumorigenicity in mice

Animal experiments were performed as described previously [56]. Five-week-old female nude mice (Experiment Animal Center of Shanghai, China) (each group, $n = 6$) were subcutaneously injected with 6×10^6 SiHa/pCon, SiHa/p63, ME-180/NC, or ME-180/shp63 cells in 0.1 ml PBS containing 20% matrigel, respectively. The growth of solid tumors of SiHa/pCon, or SiHa/p63 cells after injection was measured at the indicated time points for up to 35 days. The group of ME-180/shp63 cells tumors were measured at the indicated time points for up to 18 days. All of the animals were sacrificed and tumors were used for analysis. The tumors were calculated with caliper as previous reports [53]. All mice used in this study were treated in accordance with the National Institutes of Health Guide for the Care and Use of Laboratory Animals [57], and protocols were approved by the Institutional Animal Care and Use Committee at The University of Science and Technology of China (USTCACUC1801017). The experimental protocols did not require animal randomization. Investigators were not blinded to the experimental groups. In some cases, mice were excluded if they had unexpected deaths.

Tumor metastasis model

The immune-deficient nude mice were bred and housed in pressurized ventilated cages according to institutional regulations at University of Science and Technology of China. Experimental metastasis assays were performed using cervical cancer cell lines, SiHa/pCon, SiHa/p63, ME-180/Con, and ME-180/shp63. Cells were harvested, washed twice with PBS, and counted. A total of 6×10^6 cells were resuspended in a 0.6 ml solution of DMEM and then injected into the tail veins of 7-week-old female nude mice. All mice were in good condition after injection. At 2, 3, and 4 weeks after injection, the mice were euthanized and sacrificed. Liver and lung of each mouse were dissected for examining the metastasis tumor by H&E staining and immunohistochemistry. All mice used in this study were treated in accordance with the National Institutes of Health Guide for the Care and Use of Laboratory Animals [57], and protocols were approved by the Institutional Animal Care and Use Committee at The University of Science and Technology of China (USTCACUC1801017).

Clinical samples

The normal cervical tissues were collected from individuals between February 2007 and July 2008 as described previously [56] and all of the cervical tissue samples were obtained from the patients who were diagnosed with cervical squamous cancer staged at 1b1IIa from January 2010 to November 2016 at Anhui Provincial Hospital, Hefei, China. This study was reviewed and approved by the Ethics Review Board of Anhui Provincial Hospital. Written informed consent was obtained from each patient for this study.

Statistical evaluation

The Prism 5 (Graph Software) was used for all statistical analyses. Sample size was selected based on the ability to detect a difference of greater than 30% change at a power of 80% with $p < 0.05$. Data of all the experiments were presented as mean ± standard deviation from three biological replicates. Student's two-tailed t test or analysis of variance (ANOVA) was used to assess the statistical significance of the difference. $^*p < 0.05$, $^{**}p < 0.01$, $^{***}p < 0.001$.

Data availability

The accession number for the RNA-seq and ChIP-seq data reported in this paper is GEO: GSE135257.

Acknowledgements We would like to thank Yuhui Miao, Huimin Liu, Lu Qi, Xu Liu, Shuai Wei, Jingxin Li in University of Science and Technology of China for their valuable comments during the preparation of the manuscript. This work was supported by the National Natural Science Foundation of China (No. 81872110, 31600657, 81272881, 8137277"9, 81372777, 31725016, and 81902632); National Key Research and Development Program (2018YFC1003903); Anhui Provincial Key Research and Development Projects (1704a0802151); the Strategic Priority Research Program (Pilot study): "Biological basis of aging and therapeutic strategies" of the Chinese Academy of Sciences (grant XDPB10).

Author contributions Y.Z., G.S., X.L.W. and L.C. conceived the idea, designed the experiments, analyzed the data, wrote the paper with input from all authors and oversaw the project. F.X., L.L.Q. and J.W. performed the in vivo experiments. J.W., X.L.W. and F.X. performed the ChIP-seq, RNA-seq, qRT-PCR and analysis of the results. W.G.S. and D.Q.F. constructed the plasmids and established the stable cells. H.Y.L., Z.S., D.B.W. and B.L. performed IHC. H.Y.L. carried out most of the revision experiments. Y.Z., G.S. and L.C. wrote, reviewed, and/or revised the manuscript.

Compliance with ethical standards

Conflict of interest The authors declare that they have no conflict of interest.

Publisher's note Springer Nature remains neutral with regard to jurisdictional claims in published maps and institutional affiliations.

References

1. Minion LE, Tewari KS. Cervical cancer—State of the science: from angiogenesis blockade to checkpoint inhibition. Gynecol Oncol. 2018;148:609–21.
2. Siegel RL, Miller KD, Jemal A. Cancer statistics, 2018. CA Cancer J Clin. 2018;68:7–30.
3. Qian X, Ma C, Nie X, Lu J, Lenarz M, Kaufmann AM, et al. Biology and immunology of cancer stem(-like) cells in head and neck cancer. Crit Rev Oncol Hematol. 2015;95:337–45.
4. Rodríguez-Carunchio L, Soveral I, Steenbergen RD, Torné A, Martinez S, Fusté P, et al. HPV-negative carcinoma of the uterine cervix: a distinct type of cervical cancer with poor prognosis. BJOG. 2015;122:119–27.
5. Rusan M, Li YY, Hammerman PS. Genomic landscape of human papillomavirus-associated cancers. Clin Cancer Res. 2015;21:2009–19.
6. Rose PG, Bundy BN, Watkins EB, Thigpen JT, Deppe G, Maiman MA, et al. Concurrent cisplatin-based radiotherapy and chemotherapy for locally advanced cervical cancer. N Engl J Med. 1999;340:1144–53.
7. Sol ES, Lee TS, Koh SB, Oh HK, Ye GW, Choi YS. Comparison of concurrent chemoradiotherapy with cisplatin plus 5-fluorouracil versus cisplatin plus paclitaxel in patients with locally advanced cervical carcinoma. J Gynecol Oncol. 2009;20:28–34.
8. Yang A, Schweitzer R, Sun D, Kaghad M, Walker N, Bronson RT, et al. p63 is essential for regenerative proliferation in limb, craniofacial and epithelial development. Nature. 1999;398:714–8.
9. Candi E, Cipollone R, Rivetti di Val Cervo P, Gonfloni S, Melino G, Knight R. p63 in epithelial development. Cell Mol Life Sci. 2008;65:3126–33.
10. Mangiulli M, Valletti A, Caratozzolo MF, Tullo A, Sbisa E, Pesole G, et al. Identification and functional characterization of two new transcriptional variants of the human p63 gene. Nucleic Acids Res. 2009;37:6092–104.
11. Ying H, Chang DL, Zheng H, McKeon F, Xiao ZX. DNA-binding and transactivation activities are essential for TAp63 protein degradation. Mol Cell Biol. 2005;25:6154–64.
12. Koster MI, Roop DR. p63 and epithelial appendage development. Differentiation. 2004;72:364–70.
13. Deyoung MP, Ellisen LW. p63 and p73 in human cancer: defining the network. Oncogene. 2007;26:5169–83.
14. Chen Y, Peng Y, Fan S, Li Y, Xiao ZX, Li C. A double dealing tale of p63: an oncogene or a tumor suppressor. Cell Mol Life Sci. 2018;75:965–73.
15. Flores ER. The roles of p63 in cancer. Cell Cycle. 2007;6:300–4.
16. Mills AA. p63: oncogene or tumor suppressor? Curr Opin Genet Dev. 2006;16:38–44.
17. Fisher ML, Kerr C, Adhikary G, Grun D, Xu W, Keillor JW, et al. Transglutaminase interaction with alpha6/beta4-Integrin stimulates YAP1-dependent ΔNp63α stabilization and leads to enhanced cancer stem cell survival and tumor formation. Cancer Res. 2016;76:7265–76.
18. Salah Z, Bar-mag T, Kohn Y, Pichiorri F, Palumbo T, Melino G, et al. Tumor suppressor WWOX binds to ΔNp63α and sensitizes cancer cells to chemotherapy. Cell Death Dis. 2013;4:e480.
19. Sen T, Sen N, Brait M, Begum S, Chatterjee A, Hoque MO, et al. ΔNp63α confers tumor cell resistance to cisplatin through the AKT1 transcriptional regulation. Cancer Res. 2011;71:1167–76.
20. Chung J, Lau J, Cheng LS, Grant RI, Robinson F, Ketela T, et al. SATB2 augments ΔNp63α in head and neck squamous cell carcinoma. EMBO Rep. 2010;11:777–83.
21. Dang TT, Esparza MA, Maine EA, Westcott JM, Pearson GW. ΔNp63α promotes breast cancer cell motility through the selective activation of components of the epithelial-to-mesenchymal transition program. Cancer Res. 2015;75:3925–35.
22. Ko E, Lee BB, Kim Y, Lee EJ, Cho EY, Han J, et al. Association of RASSF1A and p63 with poor recurrence-free survival in node-negative stage I-II non-small cell lung cancer. Clin Cancer Res. 2013;19:1204–12.
23. Adorno M, Cordenonsi M, Montagner M, Dupont S, Wong C, Hann B, et al. A mutant-p53/smad complex opposes p63 to empower TGFbeta-induced metastasis. Cell. 2009;137:87–98.
24. Tran MN, Choi W, Wszolek MF, Navai N, Lee IL, Nitti G, et al. The p63 protein isoform ΔNp63α inhibits epithelial-mesenchymal transition in human bladder cancer cells: role of MIR-205. J Biol Chem. 2013;288:3275–88.
25. Dohn M, Zhang S, Chen X. p63alpha and ΔNp63α can induce cell cycle arrest and apoptosis and differentially regulate p53 target genes. Oncogene. 2001;20:3193–205.
26. Zhou Y, Xu Q, Ling B, Xiao W, Liu P. Reduced expression of ΔNp63α in cervical squamous cell carcinoma. Clin Invest Med. 2011;34:E184–91.
27. Qian L, Xu F, Wang X, Jiang M, Wang J, Song W, et al. LncRNA expression profile of ΔNp63α in cervical squamous cancers and its suppressive effects on LIF expression. Cytokine. 2017;96:114–22.
28. Lamouille S, Xu J, Derynck R. Molecular mechanisms of epithelial-mesenchymal transition. Nat Rev Mol Cell Biol. 2014;15:178–96.
29. Kalluri R, Weinberg RA. The basics of epithelial-mesenchymal transition. J Clin Invest. 2009;119:1420–8.
30. Si H, Lu H, Yang X, Mattox A, Jang M, Bian Y, et al. TNF-α modulates genome-wide redistribution of ΔNp63α/TAp73 and

NF-κB c-REL interactive binding on TP53 and AP-1 motifs to promote an oncogenic gene program in squamous cancer. Oncogene. 2016;35:5781–94.
31. Rizzo JM, Oyelakin A, Min S, Smalley K, Bard J, Luo W, et al. Delta Np63 regulates IL-33 and IL-31 signaling in atopic dermatitis. Cell Death Differ. 2016;23:1073–85.
32. Saladi SV, Ross K, Karaayvaz M, Tata PR, Mou HM, Rajagopal J, et al. ACTL6A is co-amplified with p63 in squamous cell carcinoma to drive YAP activation, regenerative proliferation, and poor prognosis. Cancer Cell. 2017;31:35–49.
33. Ortt K, Sinha S. Derivation of the consensus DNA-binding sequence for p63 reveals unique requirements that are distinct from p53. FEBS Lett. 2006;580:4544–50.
34. Gerald RC, Eric NO. NFAT signaling. Cell. 2002;109:67–79.
35. Crotti TN, Flannery M, Walsh NC, Fleming JD, Goldring SR, McHugh KP. NFATc1 regulation of the human beta (3) integrin promoter in osteoclast differentiation. Gene. 2006;372:92–102.
36. Im JY, Lee KW, Won KJ, Kim BK, Ban HS, Yoon SH, et al. DNA damage-induced apoptosis suppressor (DDIAS), a novel target of NFATc1, is associated with cisplatin resistance in lung cancer. BBA-Mol Cell Res. 2016;1863:40–9.
37. Tsukita S, Yamazaki Y, Katsuno T, Tamura A, Tsukita S. Tight junction-based epithelial microenvironment and cell proliferation. Oncogene. 2008;27:6930–8.
38. Le Bras GF, Taubenslag KJ, Andl CD. The regulation of cell-cell adhesion during epithelial-mesenchymal transition, motility and tumor progression. Cell Adh Migr. 2012;6:365–73.
39. Martin TA, Jiang WG. Tight junctions and their role in cancer metastasis. Histol Histopathol. 2001;16:1183–95.
40. Szymborska A, Gerhardt H. Hold me, but not too tight—endothelial cell–cell junctions in angiogenesis. Cold Spring Harb Perspect Biol. 2018;10:a029223.
41. Hoevel T, Macek R, Mundigl O, Swisshelm K, Kubbies M. Expression and targeting of the tight junction protein CLDN1 in CLDN1-negative human breast tumor cells. J Cell Physiol. 2002;191:60–8.
42. Lv J, Sun BH, Mai ZT, Jiang MM, Du JF. CLDN-1 promoted the epithelial to migration and mesenchymal transition (EMT) in human bronchial epithelial cells via Notch pathway. Mol Cell Biochem. 2017;432:91–8.
43. Chao YC, Pan SH, Yang SC, Yu SL, Che TF, Lin CW, et al. Claudin-1 is a metastasis suppressor and correlates with clinical outcome in lung adenocarcinoma. Am J Respir Crit Care Med. 2009;179:123–33.
44. Eftang LL, Esbensen Y, Tannaes TM, Blom GP, Bukholm IR, Bukholm G. Up-regulation of CLDN1 in gastric cancer is correlated with reduced survival. BMC Cancer. 2013;13:586.
45. Katayama A, Handa T, Komatsu K, Togo M, Horiguchi J, Nishiyama M, et al. Expression patterns of claudins in patients with triple-negative breast cancer are associated with nodal metastasis and worse outcome. Pathol Int. 2017;67:404–13.
46. Ratovitski EA. Phospho-Delta Np63 alpha regulates AQP3, ALOX12B, CASP14 and CLDN1 expression through transcription and microRNA modulation. FEBS Lett. 2013;587:3581–6.
47. Lopardo T, Lo Iacono N, Marinari B, Giustizieri ML, Cyr DG, Merlo G, et al. Claudin-1 is a p63 target gene with a crucial role in epithelial development. PLoS ONE. 2008;3:e2715.
48. Lee M, Park J. Regulation of NFAT activation: a potential therapeutic target for immunosuppression. Mol Cells. 2006;22:1–7.
49. Pflaum J, Schlosser S, Muller M. p53 family and cellular stress responses in cancer. Front Oncol. 2014;4:285.
50. Machado-Silva A, Perrier S, Bourdon JC. p53 family members in cancer diagnosis and treatment. Semin Cancer Biol. 2010;20:57–62.
51. van Bokhoven H, Brunner HG. Splitting p63. Am J Hum Genet. 2002;71:1–13.
52. Qiao F, Bowie JU. The many faces of SAM. Sci's STKE. 2005;2005:re7.
53. Zhou Y, Wei Y, Zhu J, Wang Q, Bao L, Ma Y, et al. GRIM-19 disrupts E6/E6AP complex to rescue p53 and induce apoptosis in cervical cancers. PLoS ONE. 2011;6:e22065.
54. Chen L, Rashid F, Shah A, Awan HM, Wu MM, Liu A, et al. The isolation of an RNA aptamer targeting to p53 protein with single amino acid mutation. PNAS. 2015;112:10002–7.
55. Hu S, Wang X, Shan G. Insertion of an Alu element in a lncRNA leads to primate-specific modulation of alternative splicing. Nat Struct Mol Biol. 2016;23:1011–9.
56. Zhou Y, Li M, Wei Y, Feng D, Peng C, Weng H, et al. Down-regulation of GRIM-19 expression is associated with hyperactivation of STAT3-induced gene expression and tumor growth in human cervical cancers. J Interferon Cytokine Res. 2009;29:695–703.
57. National Research Council (US). Committee for the update of the guide for the care and use of laboratory animals. guide for the care and use of laboratory animals. 8th ed. Washington, DC: National Academies Press; 2011.